Improved thermoelectric performances in textured $Bi_{1.6}Pb_{0.4}Ba_2Co_2O_y$/Ag composites

A. Sotelo, Sh. Rasekh, M. A. Torres, P. Bosque, M. A. Madre, J. C. Diez
Instituto de Ciencia de Materiales de Aragón (CSIC-Universidad de Zaragoza), Mª de Luna, 3. 50018 Zaragoza, Spain.

Abstract

$Bi_{1.6}Pb_{0.4}Ba_2Co_2O_y$ thermoelectric ceramics with small Ag additions (0, 1, and 3 wt.%) have been textured using the laser floating zone method. Microstructure has shown a slight decrease on the secondary phases content and a better grain alignment in Ag added samples. These microstructural features are reflected in the thermoelectric properties, which have shown a significant decrease of electrical resistivity, when the Ag content is raised. In spite of a corresponding decrease of Seebeck coefficient, all the Ag-containing samples possess higher Power Factor values than the $Bi_{1.6}Pb_{0.4}Ba_2Co_2O_y$ ones. Moreover, the maximum Power Factor values (about 0.36 $mW/K^2.m$ at 650 ºC) have been measured in $Bi_{1.6}Pb_{0.4}Ba_2Co_2O_y$ + 3 wt.% Ag samples, which are the best results reported in this family of materials.

Keywords: Ceramic composite; Grain growth; Texturing; Microstructure; Electrical properties

Corresponding author: A. Sotelo
e-mail: asotelo@unizar.es
Address: Dept. Ciencia de Materiales; C/Mª de Luna, 3; 50018-Zaragoza; Spain
Tel: +34 976762617
Fax: +34 976761957

1. Introduction

Due to the present and future energetic challenges, thermoelectric (TE) energy conversion can be exploited for harvesting wasted heat in the classical energy transformation systems, such as automobile, thermal power plants, etc. The use of TE systems can raise the efficiency of these systems, decreasing the fossil fuels consumption and, consequently, the release of greenhouse gases. On the other hand, for these applications TE materials with high energy conversion efficiency, quantified through the dimensionless Figure-of-Merit, ZT (= $TS^2/\rho\kappa$, where S, ρ, κ, and T, are Seebeck coefficient, electrical resistivity, thermal conductivity, and absolute temperature [1]), are necessary. Nowadays, different metallic alloys possess high performances (ZT > 1) [2] which can make them attractive for these practical applications. However, the most common, as PbTe [2] or Bi_2Te_3 [3] are based on heavy and/or toxic elements which can be oxidized or released when working at high temperatures.

In 1997, a broad research field has been opened by the discovery of relatively high thermoelectric properties in Na_xCoO_2 ceramic material (ZT ~ 0.26 at 300 K) [4]. Since then, many works have been performed on CoO-based materials with attractive thermoelectric performances [5-9]. Structural studies of these compounds have shown that their crystalline structure can be described as two different alternately stacked layers: a common conductive CdI_2-type CoO_2 layer with a two-dimensional triangular lattice, and a block layer, composed of insulating rock-salt-type (RS) layers. Both sublattices (RS block and CdI_2-type CoO_2 layer) possess common a- and c-axis lattice parameters and β angles but different b-axis length, causing a misfit along the b-direction [10,11].

The coexistence of these two sublattices produces a strong crystallographical anisotropy and anisotropic properties. As a consequence, the grains alignment is necessary when trying to achieve bulk properties close to the determined on single crystals. Among the successful techniques previously used in oxide ceramics, it is worth to mention the template grain growth (TTG) [11], sinter-forging [12], spark plasma [13], laser floating zone (LFZ) [14], or the electrically assisted LFZ [15]. On the other hand, cationic substitution has been found to be beneficial for the thermoelectric performances in previous works [16,17], leading to improved electrical behaviour. Moreover, metallic Ag additions have also

shown to enhance the thermoelectric properties of these CoO-based compounds without any evident reaction with the thermoelectric phases [18]. Taking into account previous results on textured [19], Pb doped [20], and Ag added [18] $Bi_2Ba_2Co_2O_x$ thermoelectric materials, the aim of this work is producing high performance TE materials by the simultaneous Ag addition to the optimally Pb doped $Bi_2Ba_2Co_2O_x$ compound, followed by an adequate texturing process through the well stablished LFZ technique.

2. Experimental

The initial $Bi_{1.6}Pb_{0.4}Ba_2Co_2O_y$ + x wt.% Ag (with x = 0, 1, 3, and 5) polycrystalline ceramics were prepared from commercial $Bi(NO_3)_3 \cdot 5H_2O$ (≥98 %, Aldrich), PbO (Aldrich, 99 %), $BaCO_3$ (98.5 %, Panreac), $Co(NO_3)_2 \cdot 6H_2O$ (98 %, Panreac), and metallic Ag (99 %, Aldrich) powders by a sol-gel via nitrates method. They were weighed in the appropriate proportions and dissolved in a mixture of distilled water and concentrated HNO_3 (analysis grade, Panreac). Once a clear pink solution has been obtained, citric acid (99.5 %, Panreac), and ethylene glycol (99 %, Panreac), were added to this solution in the adequate proportions. Evaporation of the solvent was slowly performed to evaporate water and decompose the nitric acid excess, increasing the pH values. The raise of pH is produced until the polymerization reaction between ethylene glycol and citric acid is started, leading to a solid pink gel [21,22] where all the cations are coordinated. Further heating at 350-400 ºC produced the organic material decomposition through a slow self combustion. The remaining powder was mechanically ground and calcined at 700 and 750 °C for 12 h, with an intermediate manual milling. This step is very important for samples textured by LFZ technique as, if barium carbonates are not totally decomposed prior texturing, they would decompose in the molten zone, leading to the solidification front destabilization. Afterwards, the resulting powders were then cold isostatically pressed in form of cylinders (~120 mm long and 2-3 mm diameter), at 200 MPa for 1 minute, which were used as feed in a LFZ system successfully applied in previous works [23]. The growth rate (30 mm/h) has been chosen to be attractive for practical applications on the basis of previous results in this system [19,24]. After the texturing process, long (more than 150 mm) cylindrical and geometrically homogeneous samples have been obtained.

The textured materials were then cut into shorter pieces with the adequate sizes for their electrical characterization (~ 15 mm long).

The structural identification of all the samples was performed by powder XRD utilizing a Rigaku D/max-B X-ray powder diffractometer (Cu Kα radiation) with 2θ ranging between 10 and 70 degrees. Microstructural observations were performed on polished samples using a Field Emission Scanning Electron Microscope (FESEM, Carl Zeiss Merlin) fitted with energy dispersive spectrometry (EDS) analysis.

Steady-state simultaneous measurements of resistivity and Seebeck coefficient were determined by the standard dc four-probe technique in a LSR-3 apparatus (Linseis GmbH) between 50 and 650ºC. From these data, PF values, as a function of temperature, were calculated in order to evaluate the thermoelectric samples performances.

3. Results and discussion

Powder XRD patterns for all $Bi_{1.6}Pb_{0.4}Ba_2Co_2O_y$ samples with different amounts of Ag are plotted (from 10 to 40° for clarity) in Fig. 1. They show very similar patterns where the most intense peaks correspond to the misfit cobaltite $Bi_{1.6}Pb_{0.4}Ba_2Co_2O_y$ phase, in agreement with previous reported data [25]. From the graph, it is clear that the cobaltite phase appears as the major one, independently of Ag content. Moreover, the peaks appearing at around 20.5 and 28.5 degrees, marked by a ✶, indicate the formation of $Bi(Pb)BaO_3$ secondary phase with $Fm\bar{3}m$ space group (#225) [26]. Furthermore, in Ag added samples a new peak appears at around 38 degrees, associated to metallic Ag (111) plane (indicated by #) [27]. This peak indicates that at least some of Ag does not react with the thermoelectric ceramic, leading to the formation of a ceramic matrix composite with metallic particles distributed inside the matrix, as observed in similar ceramic systems [28]. Moreover, from these data it is clear that the amount of secondary phases decrease with Ag addition, illustrated by the drastic decrease of the (220) peak of $(Bi,Pb)BaO_3$ phase.

SEM micrographs performed on polished longitudinal sections of all samples are shown in Fig. 2. In this figure, it can be clearly seen that all samples are composed by three main contrasts, associated through EDS to different phases.

Grey contrast (#1) corresponds to the $Bi_{1.6}Pb_{0.4}Ba_2Co_2O_y$ phase, as the major one, in agreement with the XRD data. Dark and light grey ones (#2, and #3, respectively), have been associated to $Bi_5Co_5O_{14}$, and $Bi_{1.6}Pb_{0.4}BaO_3$ secondary phases, respectively. Moreover, in the Ag added samples, a new contrast has been identified, very similar to the thermoelectric phase, as a grey one (#4 in Fig. 2d), corresponding to metallic Ag. When considering the microstructural modifications produced by Ag addition it can be observed that secondary phases content is decreased, in agreement with the XRD observations. Furthermore, the grains orientation seems to be improved with Ag addition until 3 wt.%, slightly decreasing for higher Ag proportion.

The temperature dependence of the electrical resistivity as a function of the Ag content is presented in Fig. 3. As it can be easily seen, the $\rho(T)$ curves are very similar for $Bi_{1.6}Pb_{0.4}Ba_2Co_2O_y$ samples with 0 and 1 wt.% Ag, with semiconducting-like behaviour ($d\rho/dT < 0$) in the whole measured temperature range, while for higher Ag addition, a metallic-like one ($d\rho/dT > 0$) is found between room temperature and ~ 200 ºC, changing to a slight semiconducting one at higher temperatures. Moreover, the electrical resistivity values are clearly decreased when the Ag content is increased, in the whole measured temperature range, reflecting the raise in the grain alignment and the decrease of the secondary phases content observed in the SEM micrographs. Furthermore, the lower electrical resistivity can be also reflecting an improved electrical grains connectivity promoted by Ag addition, in agreement with the microstructural observations and previously reported data [23,29], which demonstrated the formation of a ceramic-Ag composite. The minimum resistivity value at room temperature, ~ 6.5 mΩ.cm, is obtained for the $Bi_{1.6}Pb_{0.4}Ba_2Co_2O_y$ + 5 wt.% Ag samples, which is much lower than the best reported for sintered $Bi_2Ba_2Co_2O_\delta$ materials (pure and Ag-doped), typically between 550 and 21 mΩ.cm [25,30-35]. Moreover, it is also lower than the best reported values in textured $Bi_2Ba_2Co_2O_\delta$ materials, between 10-250 mΩ.cm [19,20,24,32], and very close to the values reported in single crystals (4 mΩ.cm) measured along the ab plane [36,37]. When considering the high temperature values (650 ºC), the minimum ones are measured in $Bi_{1.6}Pb_{0.4}Ba_2Co_2O_y$ + 5 wt.% Ag samples (7

mΩ.cm), much lower than the ones found in $Bi_2Ba_2Co_2O_\delta$ sintered materials (33 mΩ.cm) [30,33] or textured samples (between 8.5 and 50 mΩ.cm) [19,20,24]. Fig. 4 displays the variation of the Seebeck coefficient as a function of temperature for all the samples. In this figure, it is clear that the sign of the Seebeck coefficient is positive for the whole measured temperature range, which confirms a conduction mechanism predominantly governed by holes. Moreover, Seebeck coefficient linearly increases with temperature, which can be associated with a metal or degenerated semiconductor typical behaviour when the variation of carrier concentration, effective mass, and Fermi level with temperature are negligible. On the other hand, S values decrease with Ag content, is in agreement with the decrease of electrical resistivity. As a consequence, the maximum S value at room temperature has been determined in $Bi_{1.6}Pb_{0.4}Ba_2Co_2O_y$ samples (~ 135 μV/K), which is higher than the obtained in sintered materials (between 80 and 100 μV/K) [25,30-35], Ag doped samples (105 μV/K) [31], or single crystals (95-110 μV/K) [36,37]. Furthermore, it is comparable to the measured in textured materials (115-145 μV/K) [19,20,24,32]. The high S values found in these as-grown materials are in agreement with previous works which showed that LFZ processing of these materials generates oxygen vacancies in a larger content than in bulk sintered samples [7]. As a consequence of the necessary reduction of Co^{+4} to Co^{+3}, the holes concentration is decreased, leading to an increase of S [38], in agreement with Koshibae's expression [39]. It has already been evidenced that, when sintering under reducing atmosphere, the misfit phase $[Ca_2CoO_3][CoO_2]_{1.62}$ is not oxygen stoichiometric but contains considerable amounts of oxygen vacancies [40], explaining the high S values in these as-grown samples. When considering the values at higher temperatures, it is clear that all samples show an increase of S with temperature, reaching their maximum measured values at 650 ºC. As it was previously mentioned, the highest values at this temperature have been determined in the $Bi_{1.6}Pb_{0.4}Ba_2Co_2O_y$ samples (~ 185 μV/K, the same as in $Bi_{1.6}Pb_{0.4}Ba_2Co_2O_y$ + 1 wt.% Ag ones). These values are higher than the reported for sintered (105-120 μV/K) [30,33,35] and textured materials (145-185 μV/K) [19,20,24].

In order to evaluate the thermoelectric performances of the textured ceramic materials, PF variation with temperature has been calculated from ρ and S and displayed, as a function of the Ag content, in Fig. 5. As it can be observed in the graph, no significant modifications have been produced for the smallest Ag content (1 wt.%), in agreement with the results previously reported [18]. On the other hand, the maximum values in the whole measured temperature range have been reached for the $Bi_{1.6}Pb_{0.4}Ba_2Co_2O_y$ + 3 wt.% Ag samples, decreasing for higher Ag content. The highest PF at room temperature (0.125 mW/K^{2}m) is much higher than the reported in pure or Ag-doped sintered materials (between 0.001 and 0.035 mW/K^{2}m) [25,30-35], or most of the textured materials (0.010-0.10 mW/K^{2}m) [20,24,32]. On the other hand, it is lower than the obtained in LFZ textured materials at very low growth rates (0.15 mW/K^{2}m) [19] or single crystals (0.2-0.3 mW/K^{2}m) [36,37].

Furthermore, PF values are increased when the temperature is raised in all cases, leading to the highest measured values at 650 ºC. At this temperature, the highest determined values (0.36 mW/K^{2}m in $Bi_{1.6}Pb_{0.4}Ba_2Co_2O_y$ + 3 wt.% Ag samples) are much higher than the obtained in sintered materials (0.013-0.040 mW/K^{2}m) [30,33,35] or than the best reported in laser textured materials grown at similar rates (0.04-0.17 mW/K^{2}m) [20,24]. On the other hand, it is only slightly lower than the obtained in LFZ textured samples at very low growth rates (0.40 mW/K^{2}m in samples grown at 5 mm/h) [19].

All these data clearly show the beneficial effect promoted by the combined Pb doping and Ag addition in LFZ textured samples grown at relatively high rates, reaching PF values comparable to the obtained in materials grown at very low rates. As a consequence, these composite materials can be regarded as very attractive from the point of view of their practical applications.

4. Conclusions

This paper demonstrates that $Bi_{1.6}Pb_{0.4}Ba_2Co_2O_y$ thermoelectric materials with small Ag additions (0, 1, 3, and 5 wt.%) can be directionally grown by the laser floating zone method. It has been determined that 3 wt.% is the optimal Ag content in the $Bi_{1.6}Pb_{0.4}Ba_2Co_2O_y$ LFZ grown materials. Microstructural evolution shows that Ag slightly reduces the amount of secondary phases and improves the grain alignment. Thermoelectric data clearly show that Ag addition

significantly decreases electrical resistivity and Seebeck coefficient. The highest Power Factor values have been determined in $Bi_{1.6}Pb_{0.4}Ba_2Co_2O_y$ + 3 wt.% Ag samples at 650 ºC (~ 0.36 mW/K^2.m) which is the highest obtained in this type of materials grown at relatively high rates.

Acknowledgements

This research has been supported by the MINECO-FEDER (Project MAT2013-46505-C3-1-R). The authors wish to thank the Gobierno de Aragón (Consolidated Research Groups T87 and T12) for financial support. Authors would like to acknowledge the use of Servicio General de Apoyo a la Investigación-SAI, Universidad de Zaragoza.

References

1. D. M. Rowe, Thermoelectrics Handbook: Macro to Nano, in: D. M.Rowe (Ed.), 1st ed., CRC Press, Boca Raton, FL, 2006, pp.1-3–1-7.

2. H. Wang, J. Hwang, M. L. Snedaker, I.-H. Kim, C. Kang, J. Kim, G. D. Stucky, J. Bowers, W. Kim, High Thermoelectric Performance of a Heterogeneous PbTe Nanocomposite, Chem. Mater. 27 (2015) 944.

3. J. A. Santamaria, J. Alkorta, J. G. Sevillano, Microcompression tests of single-crystalline and ultrafine grain Bi_2Te_3 thermoelectric material, J. Mater. Res. 30 (2015) 2593.

4. I. Terasaki, Y. Sasago, K. Uchinokura, Large thermoelectric power in $NaCo_2O_4$ single crystals, Phys. Rev. B 56 (1997) 12685.

5. R. Funahashi, I. Matsubara, H. Ikuta, T. Takeuchi, U. Mizutani, S. Sodeoka, An oxide single crystal with high thermoelectric performance in air, Jpn. J. Appl. Phys. 39 (2000) L1127.

6. W. Kobayashi, S. Hebert, H. Muguerra, D. Grebille, D. Pelloquin, A. Maignan, Thermoelectric properties in the misfit-layered-cobalt oxides $[Bi_2A_2O_4]$ $[CoO_2]_{b1/b2}$ (A=Ca, Sr, Ba, b(1)/b(2)=1.65, 1.82, 1.98) single crystals. In I. Kim (Ed.), Proceedings ICT 07: Twenty-sixth international conference on thermoelectrics, Korea. 2008. pp. 117-120.

7. J. C. Diez, Sh. Rasekh, M. A. Madre, E. Guilmeau, S. Marinel, A. Sotelo, Improved Thermoelectric Properties of Bi-M-Co-O (M = Sr, Ca) Misfit

Compounds by Laser Directional Solidification, J. Electron. Mater. 39 (2010) 1601.
8. K. Rubesova, T. Hlasek, V. Jakes, S. Huber, J. Hejtmanek, D. Sedmidubsky, Effect of a powder compaction process on the thermoelectric properties of $Bi_2Sr_2Co_{1.8}O_x$ ceramics, J. Eur. Ceram. Soc. 35 (2015) 525.
9. I. V. Matsukevich, A. I. Klyndyuk, E. A. Tugova, A. N. Kovalenko, A. A. Marova, N. S. Krasutskaya, Thermoelectric properties of $Ca_{3-x}Bi_xCo_4O_{9+\delta}$ ($0.0 \leq x \leq 1.5$) ceramics, Inorg. Mater. 52 (2016) 593.
10. A. Maignan, S. Hebert, M. Hervieu, C. Michel, D. Pelloquin, D. Khomskii, Magnetoresistance and magnetothermopower properties of Bi/Ca/Co/O and Bi(Pb)/Ca/Co/O misfit layer cobaltites, J. Phys.: Condens. Matter 15 (2003) 2711.
11. H. Itahara, C. Xia, J. Sugiyama, T. Tani, Fabrication of textured thermoelectric layered cobaltites with various rock salt-type layers by using *b*-$Co(OH)_2$ platelets as reactive templates, J. Mater. Chem. 14 (2004) 61.
12. H. Wang, X. Sun, X. Yan, D. Huo, X. Li, J.-G. Li, X. Ding, Fabrication and thermoelectric properties of highly textured $Ca_9Co_{12}O_{28}$ ceramic, J. Alloys Compd. 582 (2014) 294.
13. J. G. Noudem, D. Kenfaui, D. Chateigner, M. Gomina. Toward the enhancement of thermoelectric properties of lamellar $Ca_3Co_4O_9$ by edge-free spark plasma texturing. Scripta Mater. 66 (2012) 258.
14. M. A. Madre, F. M. Costa, N. M. Ferreira, A. Sotelo, M. A. Torres, G. Constantinescu, Sh. Rasekh, J. C. Diez, Preparation of high-performance $Ca_3Co_4O_9$ thermoelectric ceramics produced by a new two-step method, J. Eur. Ceram. Soc. 33 (2013) 1747.
15. Sh. Rasekh, N. M. Ferreira, F. M. Costa, M. A. Madre, A. Sotelo, J. C. Diez, M. A. Torres, G. Constantinescu, Development of a new thermoelectric $Bi_2Ca_2Co_{1.7}O_x + Ca_3Co_4O_9$ composite, Scripta Mater. 80 (2014) 1.
16. N. Sun, S. T. Dong, B. B. Zhang, Y. B. Chen, J. Zhou, S. T. Zhang, Z. B. Gu, S. H. Yao, Y. F. Chen, Intrinsically modified thermoelectric performance of alkaline-earth isovalently substituted $[Bi_2AE_2O_4][CoO_2]_y$ single crystals, J. Appl. Phys. 114 (2013) 043705.
17. Sh. Rasekh, M. A. Madre, J. C. Diez, E. Guilmeau, S. Marinel, A. Sotelo, Effect of Pb substitution on the thermoelectrical properties of textured

$Bi_2Ca_2Co_{1.7}O_y$ ceramics prepared by a polymer solution method, Bol. Soc. Esp. Ceram. V. 49 (2010) 371.
18. Sh. Rasekh, A. Sotelo, M. A. Torres, P. Bosque, M. A. Madre, J. C. Diez, Thermoelectric properties of directionally grown $Bi_2Ba_2Co_2O_\delta$/Ag composites: Effect of annealing, J. Mater. Sci.: Mater. Electron. 2016 DOI: 10.1007/s10854-016-5435-z
19. G. Constantinescu, Sh. Rasekh, M. A. Torres, M. A. Madre, J. C. Diez, A. Sotelo, Enhancement of the high-temperature thermoelectric performance of $Bi_2Ba_2Co_2O_x$ ceramics, Scripta Mater. 68 (2013) 75.
20. M. A. Madre, F. M. Costa, N. M. Ferreira, S. I. R. Costa, Sh. Rasekh, M. A. Torres, J. C. Diez, V. S. Amaral, J. S. Amaral, A. Sotelo, High thermoelectric performance in $Bi_{2-x}Pb_xBa_2Co_2O_y$ promoted by directional growth and annealing, J. Eur. Ceram. Soc. 36 (2016) 67.
21. Z. Gaoke, L. Ying, Y. Xia, W. Yanping, O. Shixi, L. Hangxing, Comparison of synthesis methods, crystal structure and characterization of strontium cobaltite powders, Mater. Chem. Phys. 99 (2006) 88.
22. A. Sotelo, Sh. Rasekh, M. A. Madre, E. Guilmeau, S. Marinel, J. C. Diez, Solution-based synthesis routes to thermoelectric $Bi_2Ca_2Co_{1.7}O_x$, J. Eur. Ceram. Soc. 31 (2011) 1763.
23. A. Sotelo, M. A. Torres, G. Constantinescu, Sh. Rasekh, J. C. Diez, M. A. Madre, Effect of Ag addition on the mechanical and thermoelectric performances of annealed $Bi_2Sr_2Co_{1.8}O_x$ textured ceramics, J. Eur. Ceram. Soc. 32 (2012) 3745.
24. Sh. Rasekh, G. Constantinescu, M. A. Torres, M. A. Madre, J. C. Diez, A. Sotelo, Growth rate effect on microstructure and thermoelectric properties of melt grown $Bi_2Ba_2Co_2O_x$ textured ceramics, Adv. Appl. Ceram. 111 (2012) 490.
25. K. Sakai, T. Motohashi, M. Karppinen, H. Yamauchi, Enhancement in thermoelectric characteristics of the misfit-layered cobalt oxide, $[(Bi,Pb)_2Ba_{1.8}Co_{0.2}O_{4\pm\omega}]_{0.5}CoO_2$, through Pb-for-Bi substitution, Thin Solid Films 486 (2005) 58.
26. B. J. Kennedy, C. J. Howard, K. S. Knight, Z. M. Zhang, Q. D. Zhou, Structures and phase transitions in the ordered double perovskites $Ba_2Bi(III)Bi(V)O_6$ and $Ba_2Bi(III)Sb(V)O_6$, Acta Cryst. B 62 (2006) 537.

27. G. Becherer, R. Ifland, Über eine präzisionsbestimmung der gitterkonstanten von silber nach dem rückstrahlverfahren. Naturwissenschaft 41 (1954) 471.
28. D. Flahaut, J. Allouche, A. Sotelo, Sh. Rasekh, M. A. Torres, M. A. Madre, J. C. Diez, Role of Ag in textured-annealed $Bi_2Ca_2Co_{1.7}O_x$ thermoelectric ceramic, Acta Mater. 102 (2016) 273.
29. A. Sotelo, Sh. Rasekh, G. Constantinescu, M. A. Torres, M. A. Madre, J. C. Diez, Improvement of textured $Bi_{1.6}Pb_{0.4}Sr_2Co_{1.8}O_x$ thermoelectric performances by metallic Ag additions, Ceram. Int. 39 (2013) 1597.
30. H. Hao, H. Yang, Y. Liu, X. Hu, High-temperature Thermoelectric Properties of Cu-substituted $Bi_2Ba_2Co_{2-x}Cu_xO_y$ Oxides, J. Mater. Sci. Technol. 27 (2011) 525.
31. R. Ang, Y. P. Sun, X. Luo, W. H. Song, A narrow band contribution with Anderson localization in Ag-doped layered cobaltites $Bi_2Ba_3Co_2O_y$, J. Appl. Phys. 102 (2007) 073721.
32. T. Motohashi, Y. Nonaka, K. Sakai, M. Karppinen, H. Yamauchi, Fabrication and thermoelectric characteristics of $[(Bi,Pb)_2Ba_2O_{4\pm w}]_{0.5}CoO_2$ bulks with highly aligned grain structure, J. Appl. Phys. 103 (2008) 033705.
33. H. Hao, H. Yu, L. Zhao, Thermoelectric Characteristics of Pb- and La-Doped $Bi_2Ba_2Co_2O_y$ Ceramics, Adv. Mater. Res. 228-229 (2011) 804.
34. M. Hervieu, A. Maignan, C. Michel, V. Hardy, N. Creon, B. Raveau, Metallicity and thermopower of the misfit cobaltite $[Bi_2Ba_{1.8}Co_{0.2}O_4]^{RS}[CoO_2]_2$, Phys. Rev. B 67 (2003) 045112.
35. K. Sakai, M. Karppinen, J. M. Chen, R. S. Liu, S. Sugihara, H. Yamauchi, Pb-for-Bi substitution for enhancing thermoelectric characteristics of $[(Bi,Pb)_2Ba_2O_{4\pm\omega}]_{0.5}CoO_2$, Appl. Phys. Lett. 88 (2006) 232102.
36. W. Kobayashi, S. Hebert, H. Muguerra, D. Grebille, D. Pelloquin, A. Maignan, Thermoelectric properties in the misfit-layered-cobalt oxides $[Bi_2A_2O_4][CoO_2]_{b1/b2}$ (A=Ca, Sr, Ba, b1/b2=1.65, 1.82, 1.98) single crystals, Proceedings ICT'07, IEEE, Piscataway, NJ, USA, 2008, pp. 117-120.
37. X. G. Luo, H. Chen, G. Y. Wang, G. Wu, T. Wu, L. Zhao, X. H. Chen, Transport properties and magnetic-field-induced localization in the misfit cobaltite $[Bi_2Ba_{1.3}K_{0.6}Co_{0.1}O_4]^{RS}[CoO_2]_{1.97}$ single crystal, J. Phys.: Condens. Matter 20 (2008) 215221.

38. A. Maignan, D. Pelloquin, S. Hebert, Y. Klein, M. Hervieu, Thermoelectric power in misfit cobaltites ceramics: optimization by chemical substitutions, Bol. Soc. Esp. Ceram. V. 45 (2006) 122.
39. W. Koshibae, K. Tsutsui, S. Maekawa, Thermopower in cobalt oxides, Phys. Rev. B 62 (2000) 6869.
40. M. Karppinen, H. Fjellvag, T. Konno, Y. Morita, T. Motohashi, H. Yamauchi, Evidence for oxygen vacancies in misfit-layered calcium cobalt oxide, $[CoCa_2O_3]_qCoO_2$, Chem. Mater. 16 (2004) 2790.

Figure captions

Figure 1. Powder XRD diagrams for the $Bi_{1.6}Pb_{0.4}Sr_2Co_{1.8}O_x$ textured samples with a) 0; b) 1; c) 3; and d) 5 wt.% Ag. Crystallographic planes have been indicated on the peaks corresponding to the $Bi_{1.6}Pb_{0.4}Sr_2Co_{1.8}O_x$ phase. Other phases are indicated by symbols: ✶ Co-free $BiBaO_3$ secondary phase; and # Ag.

Figure 2. Scanning electron micrographs from longitudinal polished textured samples $Bi_{1.6}Pb_{0.4}Sr_2Co_{1.8}O_y$ with different Ag content: a) 0; b) 1; c) 3; and d) 5 wt.%. The different phases are indicated by arrows, 1) $Bi_{1.6}Pb_{0.4}Ba_2Co_2O_y$; 2) $Bi_5Co_5O_{14}$; 3) $Bi_{1.6}Pb_{0.4}BaO_3$; and 4) Ag.

Figure 3. Temperature dependence of electrical resistivity for textured $Bi_{1.6}Pb_{0.4}Sr_2Co_{1.8}O_x$ samples with different Ag content. ■ 0; ◆ 1; ● 3; and ▼ 5 wt.%.

Figure 4. Temperature dependence of Seebeck coefficient for textured $Bi_{1.6}Pb_{0.4}Sr_2Co_{1.8}O_x$ samples with different Ag content. ■ 0; ◆ 1; ● 3; and ▼ 5 wt.%.

Figure 5. Temperature dependence of Power Factor for textured $Bi_{1.6}Pb_{0.4}Sr_2Co_{1.8}O_x$ samples with different Ag content. ■ 0; ◆ 1; ● 3; and ▼ 5 wt.%.

Figure 1

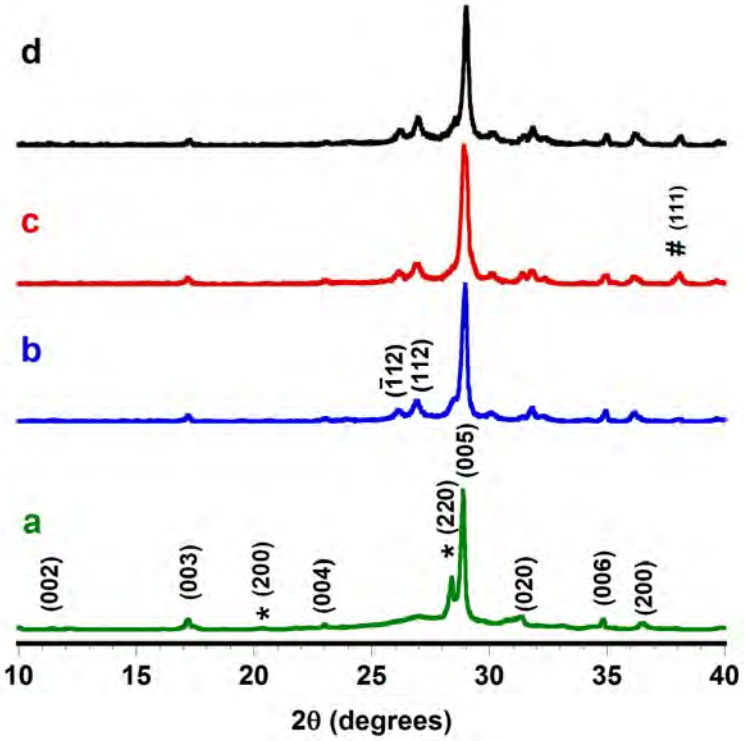
d
c
b
a
(111)
(-112)
(112)
(005)
* (220)
(002)
(003)
* (200)
(004)
(020)
(006)
(200)
10
15
20
25
30
35
40
2θ (degrees)

Figure 2

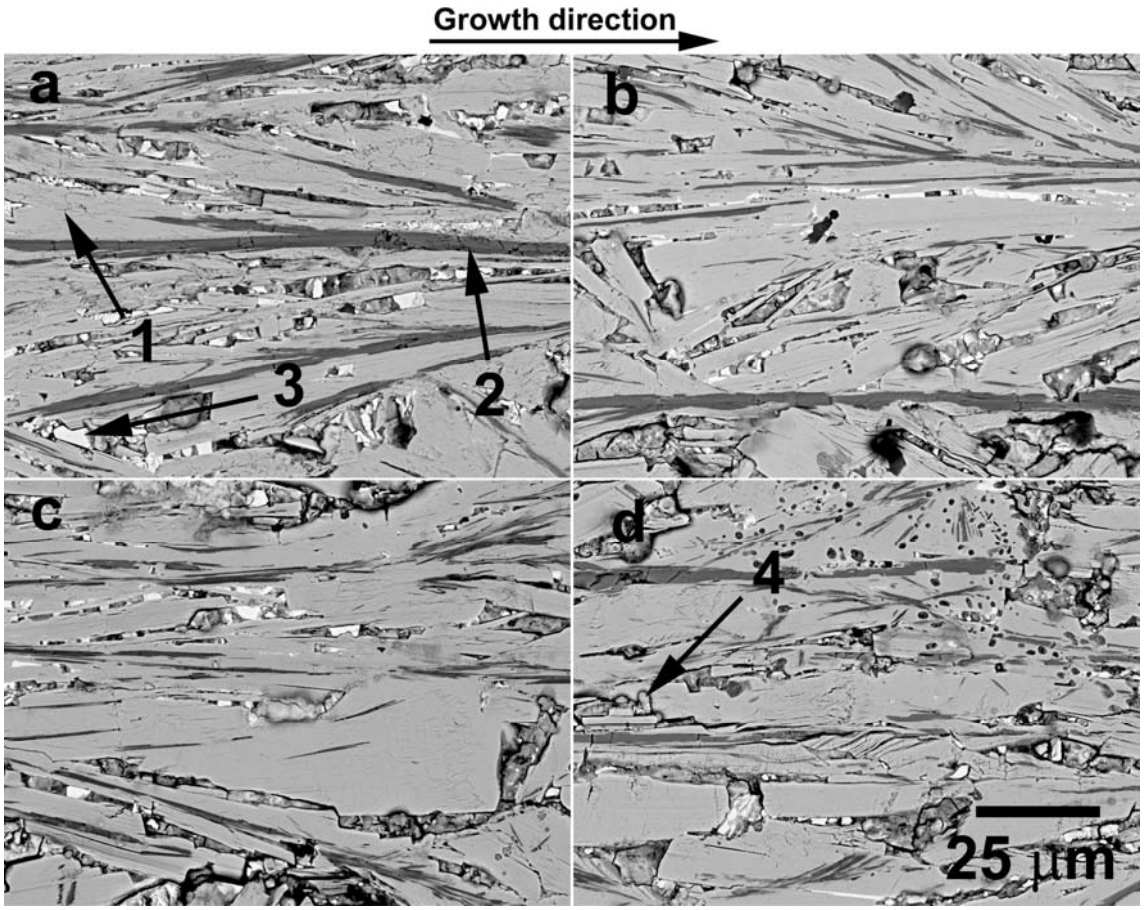

Figure 3

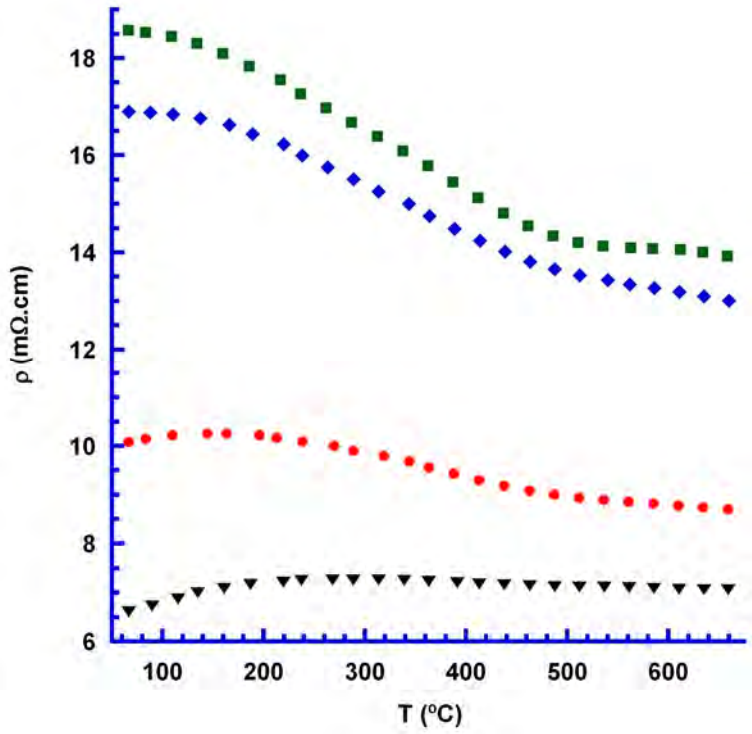

Figure 4

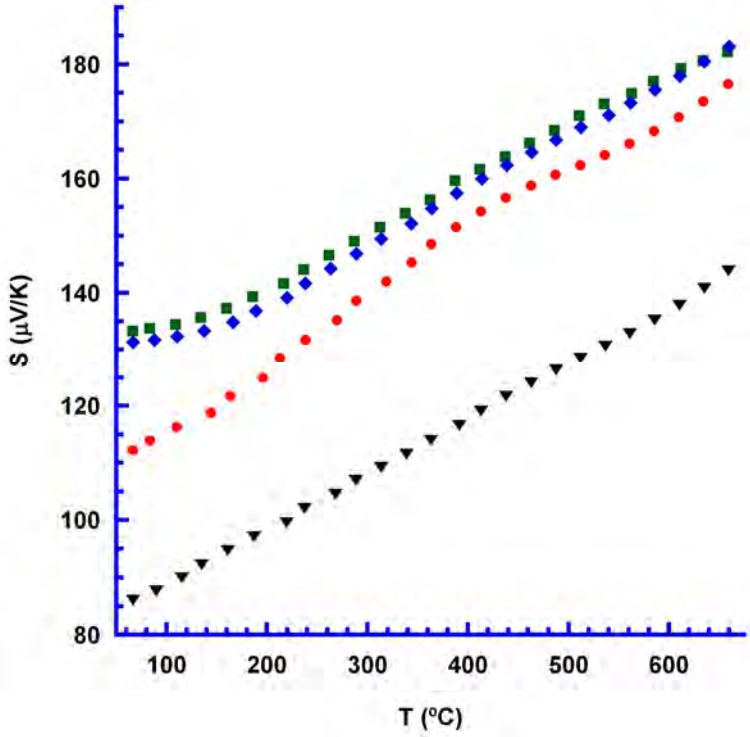

Figure 5

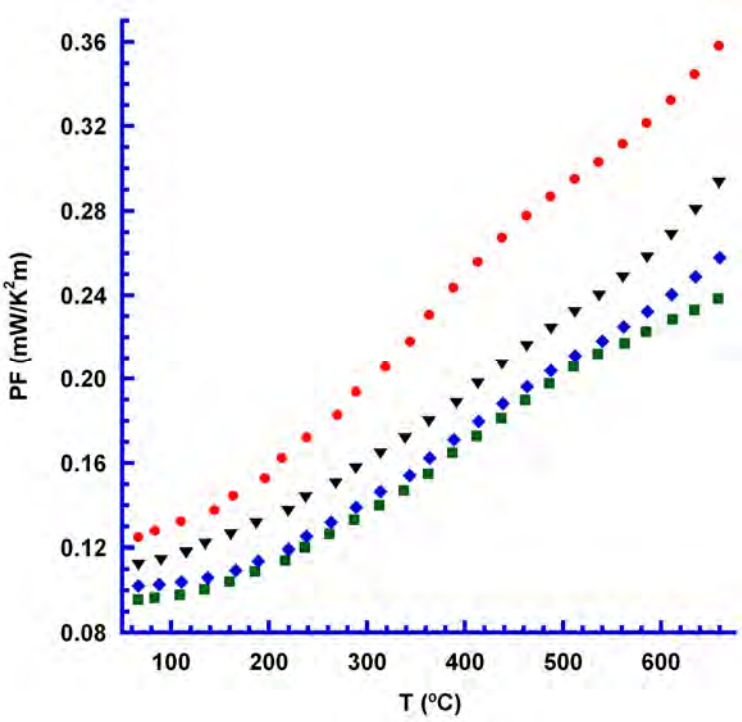
0.36
0.32
0.28
0.24
0.20
0.16
0.12
0.08
PF (mW/K²m)
100
200
300
400
500
600
T (°C)